Corrosion protection of 304L stainless steel by chemical vapor deposited alumina coatings

Ana-Maria Lazar [a,b], Wolfgang Prieto Yespica [a], Sabrina Marcelin [a], Nadine Pébère [a,*], Diane Samélor [a], Claire Tendero [a], Constantin Vahlas [a]

[a] Université de Toulouse, CIRIMAT, UPS/INPT/CNRS, ENSIACET, 4, Allée Emile Monso – BP 44362, 31030 Toulouse Cedex 4, France
[b] FCS RTRA STAE, 23 Avenue Edouard Belin, 31400 Toulouse Cedex 4, France

Keywords:
A. Stainless steel
B. EIS
B. TEM
C. Amorphous structures
C. Oxide coatings

A B S T R A C T

The corrosion protection of 304L stainless steel by aluminium oxide coatings deposited by metal–organic chemical vapor deposition (MOCVD) was investigated in a 0.1 M NaCl solution at room temperature by polarization curves and electrochemical impedance spectroscopy. The effect of the coating thickness was specifically considered. Transmission electron microscopy cross-section observations of the stainless steel/alumina coating showed that the coating is amorphous and porosity-free. The impedance response, for short immersion times, confirmed the absence of porosity and revealed that the alumina coatings with thickness ranging from 250 nm to 1700 nm provide high corrosion resistance. The corrosion protection increased when the alumina coating thickness increased. However, from the impedance data obtained for different exposure times to the aggressive solution, a threshold film thickness of 500–600 nm was determined, above which the corrosion protection was not improved. Due to their interesting physicochemical properties, such films of amorphous alumina are an innovative and economically accessible alternative to improve the stainless steel corrosion resistance and could be used in miniaturized sensors operating in marine environment.

1. Introduction

Due to their relatively good corrosion resistance, stainless steels (SSs) are foreseen as base material for the fabrication of housings of sensors which are used for the autonomous monitoring of marine environment and particularly for the measurement of parameters such as dissolved oxygen, turbidity, conductivity, pH or fluorescence. To efficiently protect the sensors, housing materials must meet multiple specifications, including resistance against corrosion, sand erosion and bio-fouling [1]. Despite the fact that the corrosion resistance of SS is improved by addition of alloying elements, still today, when exposed to chloride solutions, SS suffer from localized corrosion [2]. This situation is even worst considering the combined erosion–corrosion problem which happens when the abrasive fluid damages the passive film. The breakdown of the oxide film leads to localized corrosion propagation (intergranular or crevice corrosion) resulting in strong degradation of the SS part.

Surface treatments such as paints or coatings (organic and inorganic films) are used to face this drawback [3–6]. Ceramic films, processed either by wet techniques, such as sol–gel (titanium oxide [7]) or by vacuum techniques such as atomic layer deposition (aluminium and/or tantalum oxides [8] and their nanolaminates [9]), or microarc alloying (titanium carbide [10]) are also promising surface treatments.

Our group has recently shown that amorphous aluminium oxide coatings can be obtained through a robust, environmentally-compatible MOCVD process involving aluminium tri-isopropoxide (ATI) as single source precursor [11–13]. The processing-structure relationship was established and it revealed that deposition temperature is the key parameter of the process. When processed below 650 °C, X-ray and electron diffraction patterns showed that films are amorphous. Observation of cross-sections by transmission electron microscopy (TEM) revealed that films are compact without any visible pores. At deposition temperatures exceeding 650 °C, gradual stabilization of nanocrystallized γ-Al_2O_3 takes place. Deposition temperature also impacts the composition of the films: combined electron probe microanalysis (EPMA), Rutherford backscattering spectroscopy (RBS) and energy-dispersive X-ray spectroscopy (EDS) showed that, for films processed at 350 °C, the O/Al ratio is equal to 2. For these films, Fourier transform infrared spectrometry (FTIR) revealed the presence of OH groups, with the overall composition corresponding to that of aluminium oxy-hydroxide, AlOOH. With increasing deposition temperature, the O/Al ratio and the concentration of OH groups gradually decrease to reach a composition which matches

* Corresponding author. Tel.: +33 5 34 32 34 23; fax: +33 5 34 32 34 99.
E-mail address: Nadine.Pebere@ensiacet.fr (N. Pébère).

http://dx.doi.org/10.1016/j.corsci.2013.12.012

that of stoichiometric Al_2O_3 for films processed above 415 °C. The surface of samples processed at 480 °C is hydrophobic, with water contact angle of 103 degrees [14], and the hardness and Young's modulus are 11 GPa and 155 GPa, respectively [15].

The structure–properties relationship of such aluminium oxide coatings has been investigated on titanium alloys. Promising barrier properties against oxidation at moderate temperature (up to 650 °C; *i.e.* before crystallization of the amorphous film takes place) were shown, thus allowing the replacement of e.g. SS by titanium alloys in hotter parts of aeroturbines [15–18]. The promising performance of the amorphous alumina was attributed to the absence of grain boundaries in the coating and to the reduced oxygen vacancy diffusion in alumina [19]. Electrochemical measurements revealed that amorphous Al_2O_3 coatings processed at 480 °C provide the best performance, with a two orders of magnitude improvement of the corrosion resistance with regard to the bare titanium alloy [17].

Based on these previous results, the aim of the present work was to investigate the corrosion protection of 304L stainless steel by amorphous Al_2O_3 coatings deposited at 480 °C and to analyze the influence of the coating thickness on the corrosion performance of the coated steel. Indeed, to ensure compact coatings with acceptable corrosion protection and minimized delamination concerns, the alumina coating must be defined with a reasonable minimum thickness. The Al_2O_3 coating/stainless steel interface was examined using TEM. Polarization curves and electrochemical impedance measurements were performed for different coatings thicknesses. The corrosion protection performance of the Al_2O_3 coatings were evaluated by measuring the impedance of the samples for various exposure times (from some hours to 20 days) to a 0.1 M NaCl solution. From the capacitance values, the film thicknesses was calculated and compared to the values obtained by reflectometry measurements.

2. Experimental

2.1. MOCVD of alumina coatings

MOCVD of alumina coatings was performed from ATI in a horizontal hot-wall reactor as previously described [11]. Processing conditions were the same in all experiments: deposition temperature and pressure 480 °C and 0.67 kPa, respectively, bubbling 20 standard cubic centimetres per minute (sccm) 99.9992% pure N_2 (Air Products) flow through liquid ATI maintained at 383 K and further diluting the gas phase with additional 631 sccm N_2. These conditions lead to a theoretical flow rate of ATI between 4 and 7 sccm [20], depending on the adopted law for ATI vapor pressure provided in the literature [21–23]. The resulting growth rate of the coating was around *ca.* 12 nm/min [12]. It is worth noting that the thermal instability of the ATI molecule [12] had a negative impact on the reproducibility of the ATI flow rate, resulting in films whose thickness may be shifted with regard to the targeted one. Moreover, the N_2 bubbling technique for the production of ATI vapors was poorly adapted for short processing time and/or low film thickness compared for example with liquid injection techniques. Nevertheless, in spite of its drawbacks, this technology was adopted in the present work due to its convenient implementation at laboratory scale.

2.2. Coating deposition and characterization

The composition in weight percent of the 304L stainless steel was C = 0.02, Cr = 17–19, Ni = 9–11, Mn = 2, Si = 1, P = 0.04, S = 0.03 and Fe to balance. 10 mm x 10 mm x 1 mm plates were mechanically abraded with successive SiC papers down to 4000 grade. They were degreased and cleaned using acetone and ethanol and finally dried under Ar flow immediately before being loaded in the reactor. 250 ± 50 nm to 1700 ± 50 nm thick films were deposited on one face of the substrates by varying the deposition time. Thicker films flake off the substrate due to poor accommodation between the coefficients of thermal expansion. Film thickness was measured at different locations on the sample by reflectometry using a UV–VIS reflectometer (Ocean Optics) and the NanoCalc® software.

Scanning electron microscopy (SEM) observations of the surface of the SS and of the coatings were performed using a JEOL JSM 6400. The coating/substrate interfaces were examined by TEM. Cross-sections of the samples were prepared by cutting thin slices normal to the film/substrate interface using a diamond wire saw. Two slices were glued together, film to film, and embedded in epoxy resin in a 3 mm diameter brass tube. After curing, the tube was sectioned into approximately 300 μm thick discs. These discs were then polished on both faces and dimpled before ion-milling to transparency with a low angle (0–10°) precision ion-beam polishing system (PIPS). Observations were done with a JEOL JEM 2010 instrument operating at 200 kV and equipped with an EDS chemical analyser.

2.3. Electrochemical measurements

The electrochemical measurements were performed using a conventional three-electrode cell with bare Al (99.999 %), bare SS and alumina coated SS coupons as working electrodes, a saturated calomel reference electrode (SCE) and a platinum grid auxiliary electrode. Particular attention was paid to the preparation of the coated samples: an electrical wire was welded on the uncoated side of the SS and the entire backside of the sample including the welded zone and the edges were embedded in an insulating epoxy resin. The electrode surface of bare SS and pure Al, was polished to a 3 μm finishing with diamond paste, rinsed and sonicated with ethanol, dried in warm air and the samples were finally prepared similarly to the coated ones. To enable the comparison between the electrochemical results, the surface area in contact with the electrolyte was accurately determined by optical microscopy. The surface area varied from 0.2 cm^2 to 0.35 cm^2 depending on the sample.

Experiments were performed in a 0.1 M NaCl solution at room temperature without stirring. Polarization curves were obtained under potentiodynamic regulation using a Solartron 1287 electrochemical interface. The cathodic and anodic branches were obtained consecutively with a scan rate of 0.6 V/h after a preliminary hold time of 1 h at the corrosion potential. Electrochemical impedance measurements were carried out using a Biologic VSP instrument. The impedance diagrams were obtained under potentiostatic conditions at the corrosion potential over a frequency range between 65 kHz to a few mHz with 10 points per decade, using a 20 mV peak-to-peak sinusoidal voltage. Photographs of the coated SS surface after 20 days of immersion in a 0.1 M NaCl solution were taken by a Nikon Eclipse MA200 optical microscope.

One measurement was realized on each sample. The small surface area (<1 cm^2) and the poor statistical weight of the measurements (one measurement for each coating thickness) do not allow obtaining unambiguous quantitative information. However, the controlled and reproducible microstructure of each film allows, at least, a qualitative ranking of the samples with regard to their electrochemical behavior.

3. Results and discussion

3.1. Films characterization

Fig. 1a presents the TEM cross-section of an Al_2O_3/stainless steel interface. The film appears free of porosity in agreement with our previous results [15]. The amorphous nature of the alumina is

illustrated by the electron diffraction pattern in Fig. 1b. The film/substrate interface reveals a 15 nm thick interfacial layer (Fig. 1c) composed of Fe, Cr and Ni oxides (62% Fe, 27% Cr, 6% Ni and 5% Mn). The formation of this layer cannot be avoided as it is due to the oxidation of the SS at the beginning of the deposition process [24]. The SS oxidation stops when the Al_2O_3 layer becomes sufficiently continuous and compact.

3.2. Electrochemical results

Fig. 2 presents the polarization curves obtained in 0.1 M NaCl solution for the bare SS, for a SS sample coated with a 1500 nm thick alumina film, and for pure Al. The latter is reported for comparison with the alumina films since bare Al is naturally covered by a *ca.* 3 nm thick amorphous alumina [25]. For the three systems, the corrosion potential values account for a mixed potential linked to the simultaneous anodic and cathodic reactions occurring on their surface. In the present case, the anodic reaction is controlled by the presence of an oxide film both for the SS and for the pure Al. In neutral media, the cathodic reaction is the oxygen reduction. It can be observed that the corrosion potential of the coated SS sample is shifted towards cathodic potential (0.28 V) by comparison with the corrosion potential of the bare SS and is almost the same as that of the pure Al. For the bare SS, the cathodic part of the polarization curve is characterized by a large current plateau. On the plateau, the current density is *ca.* 30 $\mu A\ cm^{-2}$. Such low value indicates that the reaction is limited by the presence of a passive layer which impedes the electron transfer. The cathodic part of the curve obtained for the coated SS is modified by comparison with the curve obtained for the bare SS. A strong decrease of the current density (approximately three current decades) and a change in the kinetics (illustrated by an increase of the current density when the potential evolves in the cathodic direction from the corrosion potential) can be observed. The shape of the cathodic part of the curve is similar to that obtained for pure Al. The lower current densities obtained for the coated sample is attributed to the higher thickness of the alumina film. The amorphous alumina deposited on SS surface modifies the cathodic reaction due to a pronounced barrier effect which limits the oxygen reduction [17,26,27].

The anodic branch is characterized for the three systems by a passivity plateau, more or less extended in agreement with the presence of passive films on SS and Al or of the insulating alumina coating. For both the bare SS and the pure Al samples, the sharp increase of the current density is due to the breakdown of the passive film influenced by the presence of Cl^- ions in the electrolyte which induce a localized corrosion process. The values of the pitting potential; *i.e.* the potential where the localized corrosion occurs are 0.38 V/SCE and −0.1 V/SCE for SS and pure Al, respectively. The anodic domain of the coated SS is characterized by a

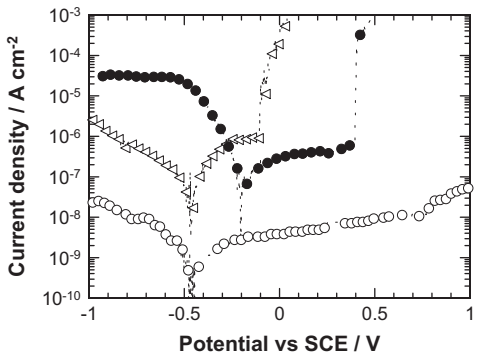

Fig. 2. Polarization curves obtained after 1 h of immersion in 0.1 M NaCl solution: (●) bare 304L SS, (△) pure Al, and (○) 304L SS coated with a 1500 nm thick alumina film.

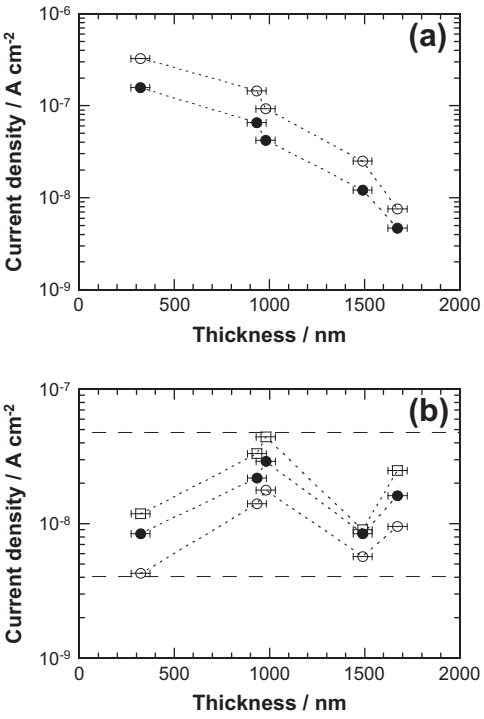

Fig. 3. Variation of the current densities as a function of the thickness of the alumina coatings: (a) for two cathodic potentials: (●) −0.8 V/SCE and (○) −0.95 V/SCE and (b) for three anodic potentials: (□) +0.5 V/SCE, (●) +0.4 V/SCE and (○) +0.2 V/SCE.

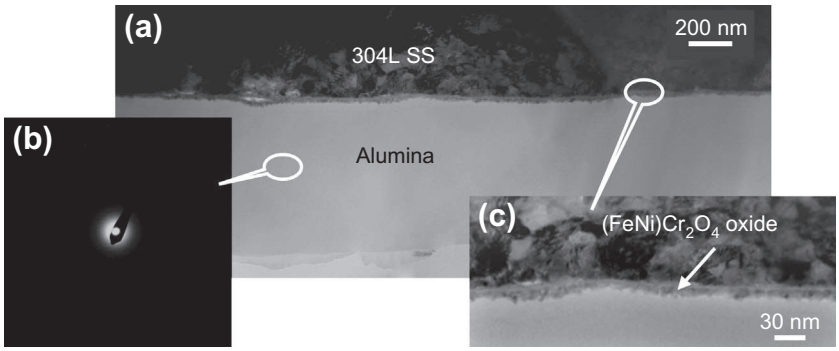

Fig. 1. (a) TEM micrograph of the Al_2O_3/stainless steel cross-section, (b) diffraction pattern of the alumina and (c) Al_2O_3/stainless steel interface.

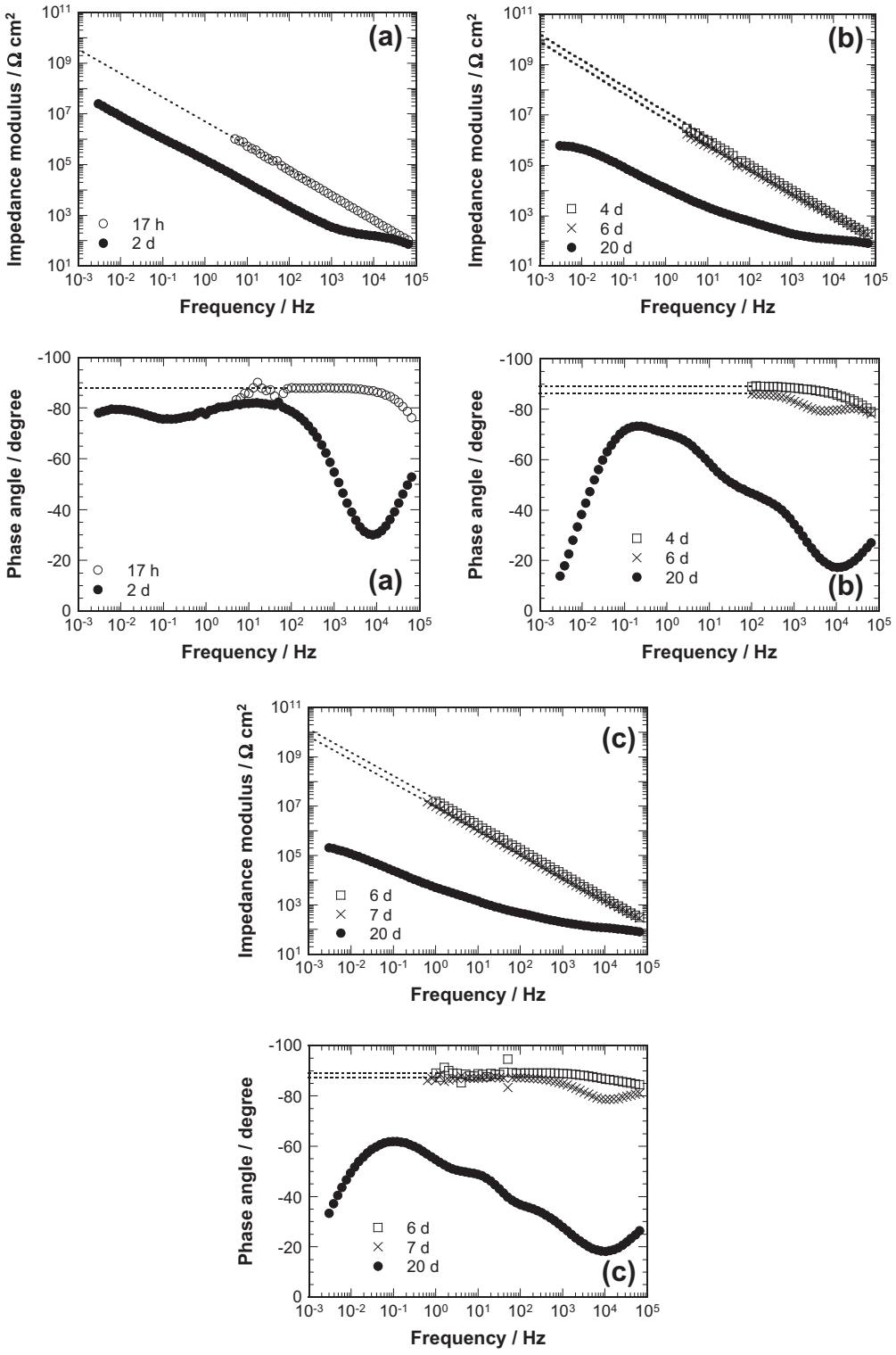

Fig. 4. Electrochemical impedance diagrams obtained at E_{corr} after different hold times in 0.1 M NaCl solution for the different alumina thicknesses: (a) 270 nm, (b) 520 nm and (c) 780 nm.

low and relatively constant current density value (about 10 nA cm^{-2}) in the whole investigated potential domain. This result underlines the stability of the coating in the aggressive medium.

The polarization curves were plotted for the SS samples coated with alumina films of various thicknesses in the range 250–1700 nm (not reported here). The curves present the same shape but the anodic and cathodic current densities depend on the thickness of the alumina coating. The current densities can provide a quantitative evaluation of the performance of the different systems [28]. In Fig. 3, the current densities are reported for different cathodic and anodic potentials for five coatings with different thicknesses. For the cathodic potentials (Fig. 3a), it can be observed that the current density significantly decreases with increasing the

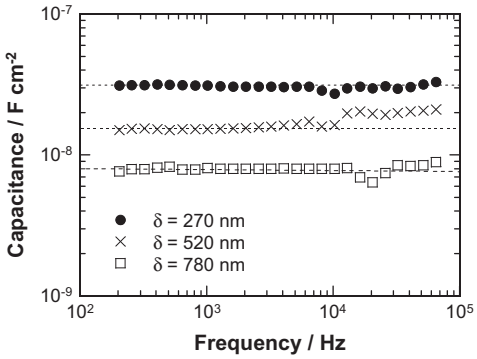

Fig. 5. Graphical determination of the alumina coating capacity before appearance of corrosion damage for the three samples after 15 h of immersion time in 0.1 M NaCl solution.

Table 1
Calculated film thickness from graphically determined capacities (considering $\varepsilon = 10$). Measured film thickness reported for comparison.

C (nF cm^{-2})	$\delta_{calculated}$ (nm)	$\delta_{measured}$ (nm)
30 ± 3	290 ± 30	270 ± 10
17 ± 1	520 ± 30	520 ± 10
9 ± 1	980 ± 110	780 ± 15

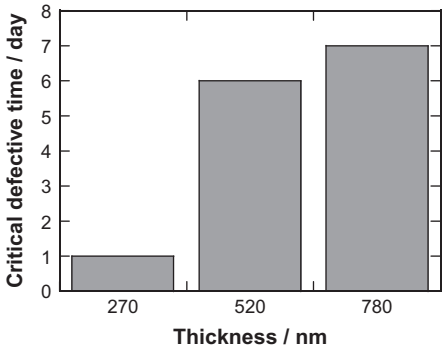

Fig. 6. Variation of CDT as a function of film thickness.

coating thickness. For 250 nm thick and for 1700 nm thick, the current densities are 1.7×10^{-7} A cm^{-2} and 4.7×10^{-9} A cm^{-2}, respectively for a cathodic potential value of −0.8 V/SCE. The decrease of the cathodic current density indicates that the rate of the oxygen reduction is reduced with increasing the coating thickness; *i.e.* with impeding the electron transfer between the metal surface and the coating/electrolyte interface [26,27]. The current densities measured on the anodic plateau for different potential values poorly depend on the coating thickness (Fig. 3b). The currents are very low (in the nA range), and thus, it can be assumed that the measured anodic currents are in the limit of the sensitivity of the potentiostat. It can be noted that the pitting potential cannot be determined in the presence of the coating indicating that most probably, thick films are less sensitive to pitting development [29,30]. In a recent paper, Diaz et al. observed, in the case of ultra-thin Al_2O_3 films (5–50 nm) deposited by atomic layer deposition, that the anodic current density decreases with increasing coating thickness [27]. Marin et al. highlighted a similar protective behavior of Al_2O_3 coatings deposited by atomic layer deposition on AISI 316 samples with thickness ranging from 10 to 100 nm [31].

Electrochemical impedance diagrams were obtained after different hold times in 0.1 M NaCl solution for three different Al_2O_3 coatings thicknesses. They are represented in Fig. 4 in Bode

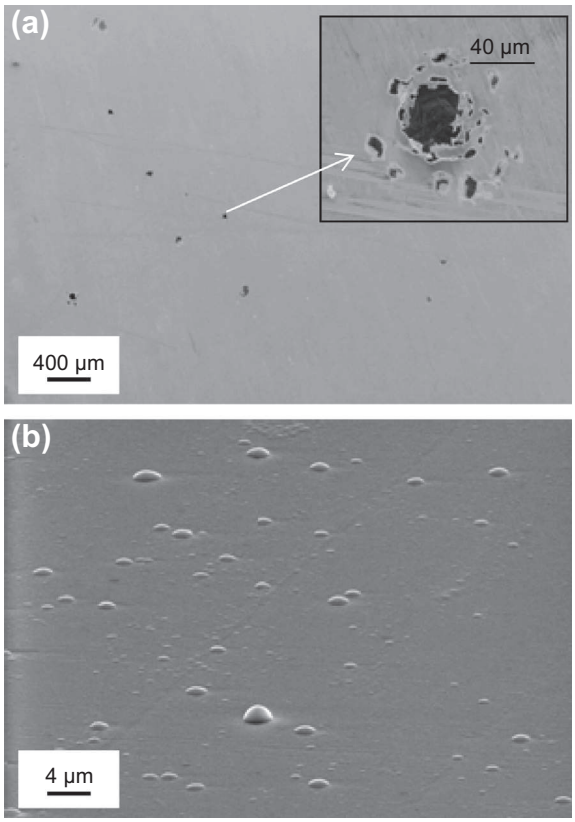

Fig. 7. SEM micrographs of the surface for (a) bare SS and (b) 1200 nm alumina coated stainless steel after 2 h of immersion in 0.1 M NaCl solution.

coordinates (modulus and phase angle as a function of frequency). Two different behaviors are observed depending on the immersion time. For short immersion times, a capacitive behavior is observed (straight line in the modulus plot and phase angle around −90°) which is characteristic of the impedance of an insulator. The impedance modulus is high and data points in the low frequency range are difficult to obtain without dispersion.

To fit the impedance data, constant phase elements (CPE) are commonly used. The CPE parameters (Q and α) can be graphically obtained [32]. In the present study, the values of α are close to 1 (0.98–0.99) for the three coatings and thus, the Q values correspond to a capacitance, expressed in unit F cm^{-2}. The C values can be obtained directly from the imaginary part of the impedance $Z_j(f)$ as:

$$C = \frac{1}{Z_j 2\pi f} \tag{1}$$

Fig. 5 shows the graphical determination of the capacitance for the three coatings. Since the impedance response can be associated to a capacitance, the dielectric constant or the film thickness may be obtained from the equation:

$$C = \frac{\varepsilon \varepsilon_0}{\delta} \tag{2}$$

where δ is the film thickness, ε is the dielectric constant and ε_0 is the permittivity of vacuum with a value of $\varepsilon_0 = 8.8542 \times 10^{-14}$ F cm^{-1}. Film thickness was calculated under the assumption that the dielectric constant ε of alumina equals 10 [33].

Table 1 compares the thickness of the three samples measured by reflectrometry and calculated from Eq. (2). The calculated values are in good agreement with the measured ones. The impedance results obtained for short immersion times showed the insulating character of the coatings which is in agreement with porosity-free films.

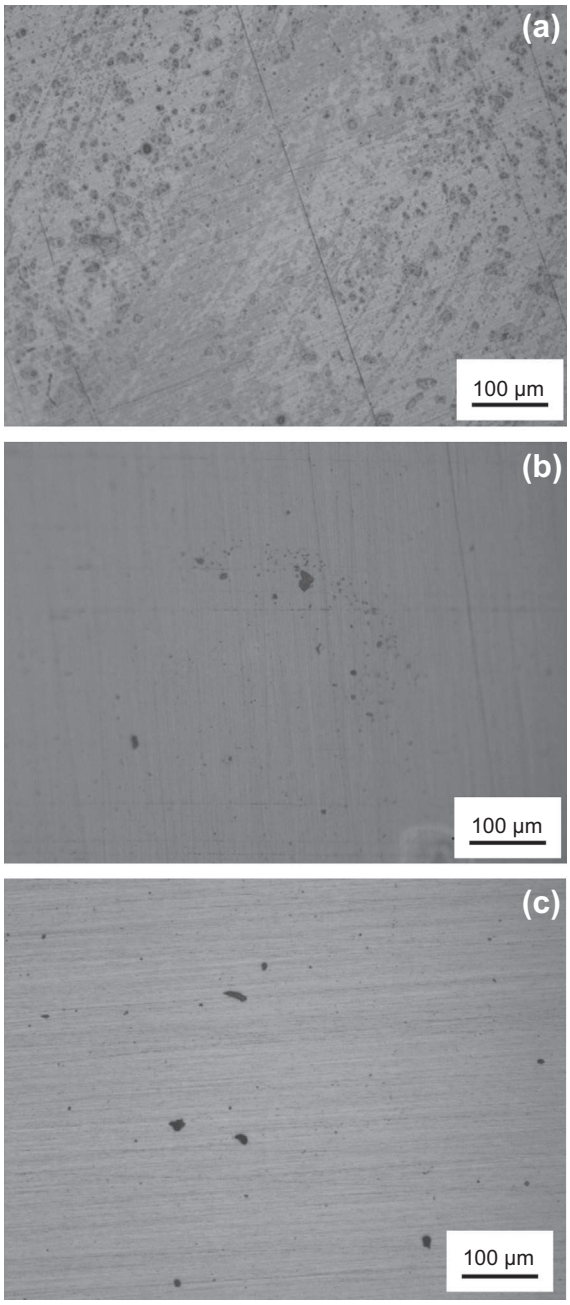

Fig. 8. Optical micrographs of the corrosion damage on Al_2O_3 coated SS after 20 days of immersion at E_{corr} in 0.1 M NaCl solution: (a) 270 nm, (b) 520 nm and (c) 780 nm.

When the immersion time increases (Fig. 4), the impedance diagrams are modified. The impedance modulus significantly decreases and the phase angle shows the presence of different time constants. This modification can be attributed to the occurrence of corrosion. However, it is difficult to extract quantitative parameters because the diagrams account both for the presence of the alumina coating and for the corrosion process. Nevertheless, it is generally accepted that the low frequency domain on the impedance diagrams characterizes the SS/coating interface and it can be assumed that the decrease of the impedance modulus with increasing immersion time is associated with the degradation of the SS/coating interface. The presence of defective sites in the coating when the exposure time to the aggressive solution is increased can explain this behavior.

Based on the above considerations, we call thereafter the immersion time corresponding to the transition between the capacitive behavior and the decrease of the impedance modulus "critical defective time" (CDT) and we use it to evaluate the corrosion protection performance of the Al_2O_3 coatings. Fig. 6 shows the CDT measured for the three coating thicknesses. It clearly appears that the thicker the coating, the longer the CDT. This result shows that the corrosion protection is improved with increasing the thickness of the alumina coating. Indeed, a significant improvement of the protection can be noticed for the 520 nm thick coating in comparison with the 270 nm thick one. The protection is not significantly improved with further increase of the thickness, as shown by the moderate increase of CDT for the 780 nm thick coating. This reveals that a threshold coating thickness is necessary to observe for a long period the protection of the SS.

3.3. Surface observations

Fig. 7 presents SEM micrographs of the surface of the bare SS and of the SS coated with a 1200 nm thick alumina film after 2 h of immersion in 0.1 M NaCl solution. For the bare SS, pits are clearly observed (Fig. 7a). The size of the pit is about 20–30 µm but probably localized corrosion propagated inside the SS as revealed by the small pits observed around the cavity (zoom in Fig. 7a). In contrast, the alumina coated sample (Fig. 7b), does not present any sign of corrosion under the same experimental conditions, which confirm its efficient protective properties.

Fig. 8 shows the micrographs, after 20 days of immersion in 0.1 M NaCl solution, of SS coated with 270 nm (8a), 520 nm (8b) and the 780 nm (8c) alumina films. For the thinner coating, the surface appears strongly corroded, in agreement with the impedance results showing that this film does not ensure long-term corrosion protection. For the thicker coatings, only some pits are visible illustrating significant improvement of the SS protection.

4. Conclusions

Polarization curves and electrochemical impedance measurements were used to assess the corrosion resistance of 304L stainless steel coated with MOCVD processed amorphous alumina films of different thicknesses. 250–1700 nm thick films provided efficient protection of SS, illustrated by a two decades reduction of the anodic current and by preventing the pitting process throughout the investigated anodic potential range. In the cathodic domain, the coated 304L SS also demonstrated a significant decrease of the current associated with the oxygen reduction. This relation between the barrier properties of the coating and its thickness was confirmed by the measure of the "Critical Defective Time", determined from impedance data, which represents the immersion time before switching from a capacitive behavior of SS/coating interface to the decrease of the impedance modulus: the higher the coating thickness, the higher the CDT (and therefore the more protective the coating). This relation is valid up to a threshold film thickness of *ca.* 500–600 nm.

The artificial passivation of 304L stainless steel with a relatively thin (*ca.* 500–600 nm) film of MOCVD amorphous alumina is an innovative and economically accessible alternative to protect it against corrosion. This work paves the way towards nanostructuring of amorphous Al_2O_3-based coatings to meet combined specifications of protection against corrosion and biofouling.

Acknowledgments

This work was supported by the Foundation for Scientific Cooperation « Sciences et Technologies pour l'Aéronautique et

l'Espace » (STAE) through the Microlaboratoires d'analyses in situ pour des observatoires environnementaux (MAISOE) project. We are indebted to Marie-Christine Lafont for TEM observations, performed at the Temscan Facility of the University of Toulouse.

References

[1] L. Delauney, C. Compère, M. Lehaitre, Biofouling protection for marine environmental sensors, Ocean Sci. 6 (2010) 503–511.
[2] T. Hong, M. Nagumo, The effect of chloride concentration on early stages of pitting for type 304 stainless steel revealed by the AC impedance method, Corros. Sci. 39 (1997) 285–293.
[3] S. Meth, N. Savchenko, F.A. Viva, D. Starosvetsky, A. Groysman, C.N. Sukenik, Siloxane-based thin films for corrosion protection of stainless steel in chloride media, J. Appl. Electrochem. 41 (2011) 885–890.
[4] Y.J. Ren, J. Chen, C.L. Zeng, Corrosion protection of type 304 stainless steel bipolar plates of proton-exchange membrane fuel cells by doped polyaniline coating, J. Power Sources 195 (2010) 1914–1919.
[5] U. León-Silva, M.E. Nicho, J.G. González-Rodríguez, J.G. Chacón-Nava, V.M. Salinas-Bravo, Effect of thermal annealing of poly(3-octylthiophene) films covered stainless steel on corrosion properties, J. Solid State Electrochem. 14 (2010) 1089–1100.
[6] C. Martinez, M. Sancy, J.H. Zagal, F.M. Rabagliati, B. Tribollet, H. Torres, J. Pavez, A. Monsalve, M.A. Paez, A zirconia-polyester glycol coating on differently pretreated AISI 316L stainless steel: corrosion behavior in chloride solution, J. Solid State Electrochem. 13 (2009) 1327–1337.
[7] H. Yun, J. Li, H.-B. Chen, C.-J. Lin, A study on the N-, S- and Cl-modified nano-TiO_2 coatings for corrosion protection of stainless steel, Electrochim. Acta 52 (2007) 6679–6685.
[8] S.E. Potts, L. Schmalz, M. Fenker, B. Díaz, J. Światowska, V. Maurice, A. Seyeux, P. Marcus, G. Radnóczi, L. Tóth, W.M.M. Kessels, Ultra-thin aluminium oxide films deposited by plasma-enhanced atomic layer deposition for corrosion protection, J. Electrochem. Soc. 158 (2011) C132–C138.
[9] E. Harkonen, B. Diaz, J. Swiatowska, V. Maurice, A. Seyeux, M. Vehkamäki, T. Sajavaara, M. Fenker, P. Marcus, M. Ritala, Corrosion protection of steel with oxide nanolaminates grown by atomic layer deposition, J. Electrochem. Soc. 158 (2011) C369–C378.
[10] Y.J. Ren, C.L. Zeng, Corrosion protection of 304 stainless steel bipolar plates using TiC films produced by high-energy micro-arc alloying process, J. Power Sources 171 (2007) 778–782.
[11] A. Gleizes, C. Vahlas, M.M. Sovar, D. Samélor, M.C. Lafont, Chemical vapor deposited aluminium oxide coatings from aluminium tri-iso-propoxide: correlation between processing conditions and composition, Chem. Vap. Dep. 13 (2007) 23–29.
[12] M.M. Sovar, D. Samélor, A.N. Gleizes, C. Vahlas, Aluminium tri-isopropoxide: shelf life, transport properties, and decomposition kinetics for the low temperature processing of aluminium oxide-based coatings, Surf. Coat. Technol. 201 (2007) 9159–9162.
[13] H. Vergnes, D. Samelor, A. Gleizes, C. Vahlas, B. Caussat, Local kinetic modeling of aluminium oxide metal organic chemical vapor deposition from aluminium tri-isopropoxide, Chem. Vap. Dep. 17 (2011) 181–185.
[14] D. Samélor, A.M. Lazar, M. Aufray, C. Tendero, L. Lacroix, J.D. Béguin, B. Caussat, H. Vergnes, J. Alexis, D. Poquillon, N. Pébère, A. Gleizes, C. Vahlas, Amorphous alumina coatings: processing, structure and remarkable barrier properties, J. Nanosci. Nanotechnol. 11 (2011) 8387–8391.
[15] Y. Balcaen, N. Radutoiu, J. Alexis, J.D. Béguin, L. Lacroix, D. Samelor, C. Vahlas, Mechanical and barrier properties of MOCVD processed alumina coatings on TA6V titanium alloy, Surf. Coat. Technol. 206 (2011) 1684–1690.
[16] J.D. Béguin, D. Adrian, J.A. Petit, J.P. Rivière, C. Vahlas, S. Vaillant, Improvement of salt corrosion resistance of titanium alloys by PVD and CVD coatings, Surface Modification Technologies XX (2006) 59–63.
[17] G. Boisier, M. Raciulete, D. Samélor, N. Pébère, A.N. Gleizes, C. Vahlas, Electrochemical behavior of chemical vapor deposited protective aluminium oxide coatings on Ti6242 titanium alloy, Electrochem. Sol. State Lett. 11 (2008) C55–C57.
[18] D. Samélor, M. Aufray, L. Lacroix, Y. Balcaen, J. Alexis, H. Vergnes, D. Poquillon, J.D. Beguin, N. Pébère, S. Marcelin, B. Caussat, C. Vahlas, Mechanical and surface properties of chemical vapour deposited protective aluminium oxide films on TA6V alloy, Adv. Sci. Technol. 66 (2010) 66–73.
[19] U. Aschauer, P. Bowen, S.C. Parker, Oxygen vacancy diffusion in alumina: new atomistic simulation methods applied to an old problem, Acta Mater. 57 (2009) 4765–4772.
[20] S.D. Hersee, J.M. Ballingall, The operation of metalorganic bubblers at reduced pressure, J. Vac. Sci. Technol. A8 (1989) 800–804.
[21] R.H.T. Bleyerveld, W. Fieggen, H. Gerding, Structure and physical properties of aluminium alkoxides. Part IV: Vapor-pressures of aluminium isopropoxide, Rec. Trav. Chim. Pays-Bas 91 (1972) 477–482.
[22] R.C. Mehrotra, Aluminium alkoxides, J. Indian Chem. Soc. 30 (1953) 585–591.
[23] K.J. Sladek, W.W. Gibert, Low temperature metal oxide deposition by alkoxide hydrolysis, in: F.A. Glaski (Ed.) 3rd Int. Conf. CVD, The American Nuclear Society, Hinsdale, IL, The University of Utah, Salt Lake City, Utah, 1972, pp. 215–231.
[24] S. Cissé, L. Laffont, B. Tanguy, M.-C. Lafont, E. Andrieu, Effect of surface preparation on the corrosion of austenitic stainless steel 304L in high temperature steam and simulated PWR primary water, Corros. Sci. 56 (2012) 209–216.
[25] L.P.H. Jeurgens, W.G. Sloof, F.D. Tichelaar, C.G. Borsboom, E.J. Mittemeijer, Determination of thickness and composition of aluminium-oxide overlayers on aluminium substrates, Appl. Surf. Sci. 144–145 (1999) 11–15.
[26] B. Diaz, E. Härkönen, J. Swiatowska, V. Maurice, A. Seyeux, P. Marcus, M. Ritala, Low-temperature atomic layer deposition of Al_2O_3 thin coatings for corrosion protection of steel: surface and electrochemical analysis, Corros. Sci. 53 (2011) 2168–2175.
[27] B. Diaz, J. Swiatowska, V. Maurice, A. Seyeux, B. Normand, E. Harkonen, M. Ritala, P. Marcus, Electrochemical and time of flight secondary ion mass spectrometry analysis of ultra-thin metal oxide (Al_2O_3 and Ta_2O_5) coatings deposited by atomic layer depostion on stainless steel, Electrochim. Acta 56 (2011) 10516–10523.
[28] M. Kendig, A. Davenport, H. Isaacs, The mechanism of corrosion inhibiton by chromate conversion coatings from X-ray absorption near edge spectroscopy (XANES), Corros. Sci. 34 (1993) 41–49.
[29] S.-I. Pyun, W.-J. Lee, The effect of prior Cl^- ion incorporation into native oxide film on pure aluminium in neutral chloride solution on pit initiation, Corros. Sci. 43 (2001) 353–363.
[30] E. McCafferty, The electrode kinetics of pit initiation on aluminum, Corros. Sci. 37 (1995) 481–492.
[31] E. Marin, L. Guzman, A. Lanzutti, W. Ensinger, L. Fedrizzi, Multilayer Al_2O_3/TiO_2 Atomic Layer Deposition coatings for the corrosion protection of stainless steel, Thin Solid Films 552 (2012) 283–286.
[32] M.E. Orazem, N. Pébère, B. Tribollet, Enhanced graphical representation of electrochemical impedance data, J. Electrochem. Soc. 153 (2006) B129–B136.
[33] W.M. Haynes, CRC Handbook of Chemistry and Physics, in, Taylor and Francis Group, LLC, New York, NY, 2012.